Research paper

# *In silico* non-liner dynamic analysis reflecting *in vitro* physical properties of CAD/CAM resin composite blocks

Dr. Oğuzcan Karaer[a], DDS, Dr. Satoshi Yamaguchi[b]*, Ph.D., Dr. Yutaro Nakase[b,c], DDS, Dr. Chunwoo Lee[b], DDS, Prof. Satoshi Imazato[b, d], DDS, Ph.D.

[a] Department of Prosthodontics, Faculty of Dentistry, Ankara University, Ankara 06560, Turkey

[b] Department of Biomaterials Science, Osaka University Graduate School of Dentistry, 1-8 Yamadaoka, Suita, Osaka 565-0871, Japan

[c] Department of Pediatric Dentistry, Osaka University Graduate School of Dentistry, 1-8 Yamadaoka, Suita, Osaka 565-0871, Japan

[d] Department of Advanced Functional Materials Science, Osaka University Graduate School of Dentistry, 1-8 Yamadaoka, Suita, Osaka 565-0871, Japan

* Correspondence should be addressed to Satoshi Yamaguchi

Department of Biomaterials Science, Osaka University Graduate School of Dentistry

1-8 Yamadaoka, Suita, Osaka 565-0871, Japan

Tel/Fax: +81-6-6879-2917

E-mail: yamagu@dent.osaka-u.ac.jp

## Abbreviations

| | |
|---|---|
| CAD/CAM | Computer-aided design/computer-aided manufacturing |
| NTP | Notchless triangular prism |
| FEA | Finite element analysis |
| SEM | Scanning electron microscopy |

## ABSTRACT

***Purpose.*** The aim of this study was to assess the validity of *in silico* models of three-point bending tests to reflect *in vitro* physical properties obtained from three commercially available computer-aided design/computer-aided manufacturing (CAD/CAM) resin composite blocks and demonstrate notchless triangular prism analysis with those properties.

***Material and Methods*.** Three types of commercially available CAD/CAM resin composite blocks were used: Cerasmart 300 (CS300; GC, Tokyo, Japan), Katana Avencia P Block (AP; Kuraray Noritake Dental, Tokyo, Japan), and KZR CAD HR3 Gamma Theta (GT; Yamakin, Osaka, Japan). *In vitro*/*in silico* three-point bending tests were conducted to obtain elastic modulus and fracture strain for nonlinear dynamic finite element analysis (n=10/each). Fractured surfaces of specimens after *in vitro* NTP tests were observed, and the fracture toughness of each CAD/CAM resin composite was obtained by *in silico* NTP analysis.

***Results*.** Both *in vitro* and *in silico* load–displacement curves obtained from three-point bending tests were significantly correlated ($p < 0.05$). The elastic moduli of CS300, AP, and GT were 8.0 GPa, 10.0 GPa, and 9.0 GPa, respectively. The fracture toughness values obtained from *in silico* NTP analysis of CS300, AP, and GT were 5.057 $MPa \cdot m^{1/2}$, 4.193 $MPa \cdot m^{1/2}$, and 4.880 $MPa \cdot m^{1/2}$, respectively. There was no significant difference in the length of the stable region among the three CAD/CAM resin composites ($p = 0.09$).

***Conclusions.*** The *in silico* approach established in this study showed acceptable reflection of *in vitro* physical properties and will be useful for assessing fracture toughness related to the longevity of CAD/CAM resin composites without wastage of materials.

**KEYWORDS**: Resin composites, Fracture toughness, Finite element analysis, Computer aided design, Computer aided manufacturing

## 1. INTRODUCTION

Computer-aided design/computer-aided manufacturing (CAD/CAM) resin composite blocks are esthetic restorative materials and may possibly be used as an alternative to metals or ceramics (Ruse and Sadoun, 2014). CAD/CAM resin composite blocks have greater mechanical properties than conventional filling resin composites because of their highly dense nanofillers (Coldea et al., 2013a, b; Okada et al., 2014) and pre-polymerization procedures (Nguyen et al., 2012, 2013). After approval by Japanese health insurance companies in 2014, clinical treatment with CAD/CAM resin composites in the molar region have steadily increased. However, the longevity of CAD/CAM resin composite molar crowns is still unknown (Yamaguchi et al., 2018a).

The fracture toughness of resin composites is one key criterion for evaluating resistance to crack propagation from the existing initiation points related to the fatigue performance of CAD/CAM resin composites. Additionally, a significant weak correlation between wear performance and clinical fractures relating to the fracture toughness has been reported (Heintze et al., 2017). The single-edge notched beam and the chevron notch short rod/beam tests are available to evaluate the fracture toughness of dental materials (Fujishima and Ferracane, 1996; Ilie et al., 2012; Ornaghi et al., 2014; Tantbirojn et al., 2003). However, it is difficult to reproduce the shape of the notch, making the specimen preparation challenging.

77 Notchless triangular prism (NTP) tests have been proposed by Ruse *et al*. (Ruse et al.,
78 1996) as a simpler method to evaluate both the fracture toughness of materials and bonded
79 interfaces between the adhesive and restorative materials (Eldafrawy et al., 2018; Mesmar and
80 Ruse, 2019). Tensile stress calculated by finite element analysis (FEA) using the NTP test and
81 the chevron notch short rod test showed no differences in distribution (Ruse et al., 1996).
82 FEA is well established as a method for assessing stress distribution, and is useful for
83 investigating fracture initiation points in dental materials (Ausiello et al., 2004; Coelho et al.,
84 2008; Dal Piva et al., 2018; Della Bona et al., 2013; Yamaguchi et al., 2018a; Yamanishi et al.,
85 2014). It is difficult to determine which is the best composition of CAD/CAM resin composites
86 to optimize fracture toughness, and *in vitro* fracture toughness tests are still conducted by using
87 actual specimens. *In vitro* experimental results involve complex factors such as shape, size,
88 materials, layout of fillers, and coupling conditions between fillers and the resin matrix
89 (Ferracane, 2011). One of the advantages of FEA is the ability to evaluate the stress distribution
90 focusing on specific factors related to mechanical performance (Yamaguchi et al., 2017). This
91 feature makes FEA a particularly useful tool in materials design.
92 Non-linear dynamic FEA can represent fracture propagation corresponding to the
93 fracture criteria of materials, as well as the stress distributions (Yamaguchi et al., 2014).
94 Fracture criteria are important factors for obtaining accurate fracture loads reflecting the *in vitro*

results. The maximum principal strain has been reported as the best fracture criterion for evaluating the flexural strength of resin composites (Yamaguchi et al., 2018b). The combination of nonlinear dynamic FEA and the fracture criterion makes it possible to develop *in silico* models of NTP tests to reflect the *in vitro* results.

The aim of this study was to assess the validity of *in silico* models of three-point bending tests to reflect *in vitro* physical properties obtained from three commercially available CAD/CAM resin composite blocks and demonstrate notchless triangular prism analysis with those properties.

## 2. Materials and methods

### 2.1 CAD/CAM resin composites blocks

Three types of commercially available CAD/CAM resin composites blocks were used: Cerasmart 300 (CS300; GC, Tokyo, Japan), Katana Avencia P Block (AP; Kuraray Noritake Dental, Niigata, Japan), and KZR CAD HR3 Gamma Theta (GT; Yamakin, Osaka, Japan). Details of the material composition of each block are summarized in Table 1.

Table 1. Composition of CAD/CAM resin composites used in this study

| | Code | Manufacturer | Filler and monomer | Filler content (wt%) |
|---|---|---|---|---|
| Cerasmart 300 | CS300 | GC | Barium glass, silica powder<br>UDMA, Bis-MEPP, polyfunctional methacrylate | 78 |
| Katana Avencia P Block | AP | Kuraray Noritake Dental | Mixed filler with silanated barium glass, silanated colloidal silica,<br>Cured resins consisting of methacrylate monomer, UDMA | 82 |
| KZR-CAD HR3 Gamma Theta | GT | YAMAKIN | Inorganic oxide filler, fluoride-releasing filler, spherical nanofiller ($SiO_2$)<br>Methacrylate monomer | 75 |

### 2.2 *In vitro*/*in silico* three-point bending tests

*In vitro* three-point bending tests were conducted using each material (4.0 × 1.2 × 14.0 mm specimen, n = 10) after storage in water for 24 hours using a universal testing machine (EZ-SX, Shimadzu, Kyoto, Japan) with a 1.0 mm/min cross head speed. The obtained load–displacement curve was converted into a stress–strain curve. The flexural modulus was obtained from the initial slope of the stress–strain curve, and the fracture strain was recorded at the end

of the curve. Micro computed tomography (micro-CT; R_mCT2, Rigaku, Tokyo, Japan) analysis for calculating the volume and the weight measurement of each specimen were conducted to calculate densities. Using the data obtained by these *in vitro* tests, the elastic modulus of each material was obtained by *in silico* non-linear dynamic FEA (LS-DYNA, LSTC, Livermore, CA, USA). The flexural modulus and the elastic modulus are not equal. The flexural modulus was used as an initial elastic modulus for three-point bending analysis. After the first analysis, there is some difference between *in vitro* and *in silico* load displacement curve. Until converging those curves, the analysis was repeatedly conducted. Finally, the elastic modulus of each material was determined. The Poisson's ratio of each material was set to 0.38 according to that of dental composites (Greaves et al., 2011).

### 2.3 Specimen preparation and *in vitro* notchless triangular prism tests

For the notchless triangular prism (NTP) test, 6 × 6 × 6 × 12 mm specimens were prepared by milling machine (DWX-51D, Roland DG, Hamamatsu, Japan) and polished with #2000 SiC paper. All the specimens were immersed into 37ºC water for 24 hours. A fracture initiation point 0.1 mm in depth was opened on the middle edge of the triangular prism specimen using a stainless steel razor blade using custom-made jigs (TRUE SEED, Kyoto, Japan). The edge of the triangular specimens was carefully observed under an optical

135 microscope (HM-211, Mitsutoyo, Kawasaki, Japan) with 10× magnification. The specimens
136 were wiped and fixed on custom-made jigs for the NTP tests (TRUE SEED). The NTP tests
137 were conducted with a universal testing machine (EZ-SX, Shimadzu, Kyoto, Japan) with a 1.0
138 mm/min crosshead speed.
139
140 The fractured surfaces of the specimens were then gold-coated using Quick Coater (SC-
141 701, Sanyu Electron, Tokyo, Japan) and observed by scanning electron microscopy (SEM;
142 JSM-6390BU, JEOL, Tokyo, Japan) under 30× magnification at 5 kV. The length from the
143 crack initiation point to the boundary between the stable and unstable regions was measured
144 using Image J software (National Institute of Health, Bethesda, MD, USA).
145
146 **2.4 *In silico* notchless triangular prism analysis**
147 Using the elastic moduli and fracture strains obtained from *in vitro* three-point bending
148 tests and densities, NTP analysis was conducted by *in silico* non-linear dynamic FEA using the
149 same CAD models designed for the custom-made jigs for the NTP tests (Fig. 1). The fracture
150 toughness ($K_{1c}$) of each model was calculated using the following equation:
151

$$K_{1C} = \frac{P}{D\sqrt{W}} Y_{\min}$$

152 ,

where $P$ is the load at fracture, $D$ (12.0 mm) is the length of the prism, $W$ (10.5 mm) is the length of the mold, and $Y_{min}$ (28.0) is the stress intensity factor.

The maximum principal strain distribution was obtained once there was 0.1 mm displacement until fracture.

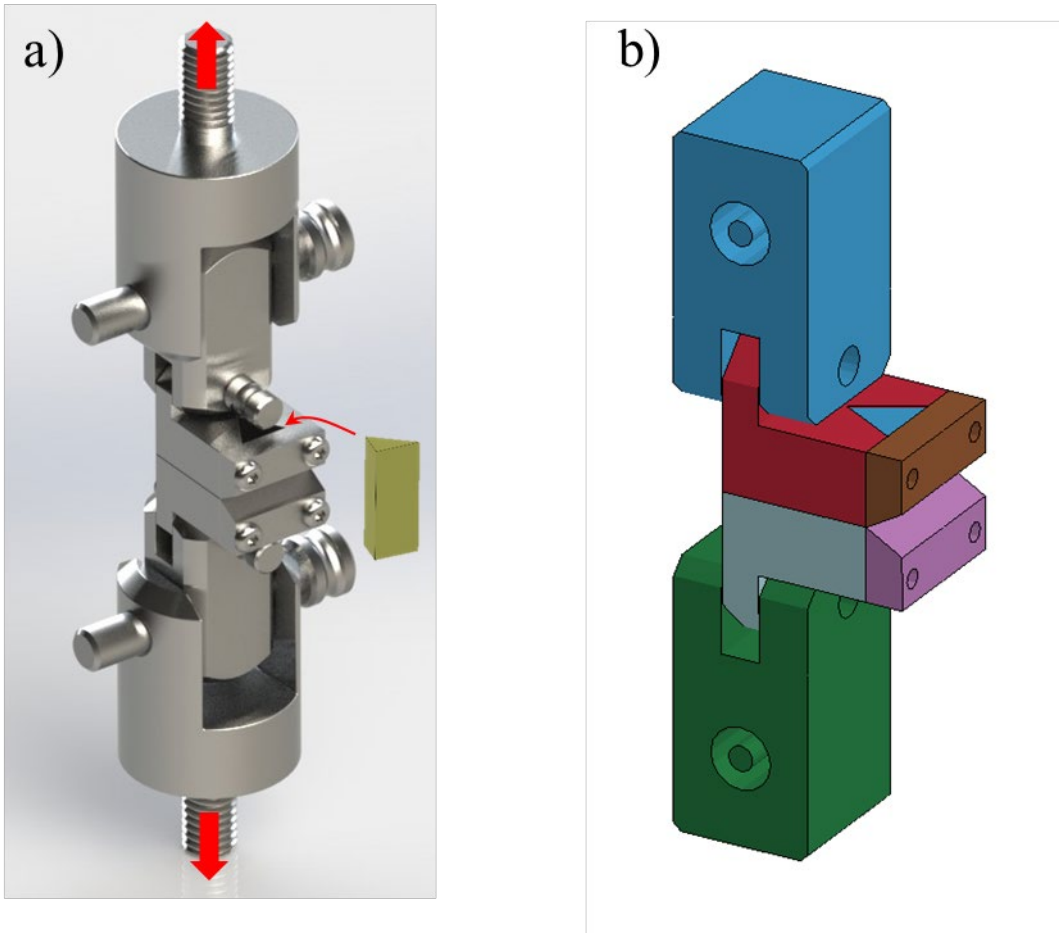


**Fig. 1** CAD models for NTP tests. **a** CAD models of *in vitro* NTP tests for fabricating custom-made jigs. **b** CAD models for *in silico* NTP analysis.

## 2.5 Statistical analysis

Loads at each time point obtained from the *in vitro* three-point bending tests were compared statistically with the value determined by *in silico* analysis using Pearson's correlation tests (PASW Statistics 18, IBM, Somers, NY, USA). Additionally, loads at each time point obtained from the *in vitro* NTP tests were compared statistically with the value determined by *in silico* analysis using Spearman's correlation test.

The lengths of stable region obtained from the SEM images were compared statistically using one-way analysis of variance (ANOVA) with Tukey's post hoc test.

*P*-values of less than 0.05 were considered as statistically significant for all tests.

## 3. RESULTS

### 3.1 Elastic moduli obtained from *in silico* three-point bending analysis

The flexural moduli, densities, and fracture strains of CS300, AP, and GT are summarized in Table 2. *In vitro* / *in silico* load–displacement curves after the three-point bending tests/analysis are shown in Figure 2. The *in vitro* curve was obtained by averaging all loads at each time point. Both *in vitro* and *in silico* load–displacement curves were significantly correlated (CS300: R=0.99, AP: R=1.0, GT: R=0.99, $p < 0.05$). The elastic moduli of CS300, AP, and GT were 8.0 GPa, 10.0 GPa, and 9.0 GPa, respectively.

Table 2. Physical properties of CAD/CAM resin composites obtained by *in vitro* three-point bending tests, micro-CT analysis, and weight measurement

| | Flexural modulus (GPa) | Density (g/cm$^3$) | Fracture strain (ε) |
|---|---|---|---|
| CS300 | 6.765 ± 1.042 | 2.17 ± 0.00682 | 0.0366 ± 0.00627 |
| AP | 9.261 ± 1.774 | 2.35 ± 0.00994 | 0.0247 ± 0.00267 |
| GT | 7.424 ± 1.053 | 2.08 ± 0.00364 | 0.0322 ± 0.00346 |

a)

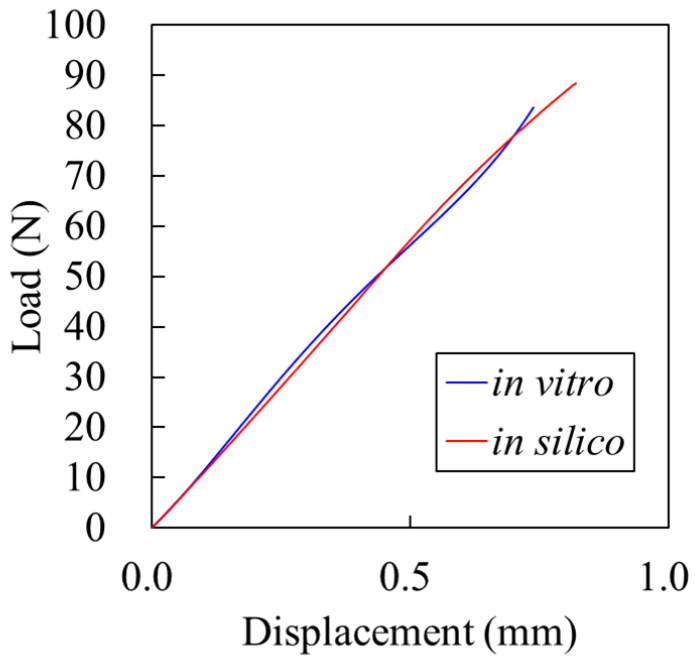


183

b)

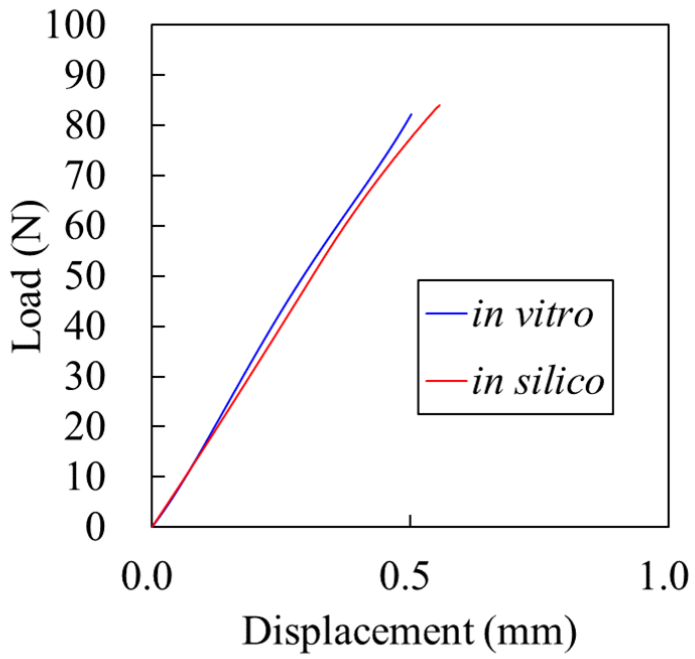


184

185

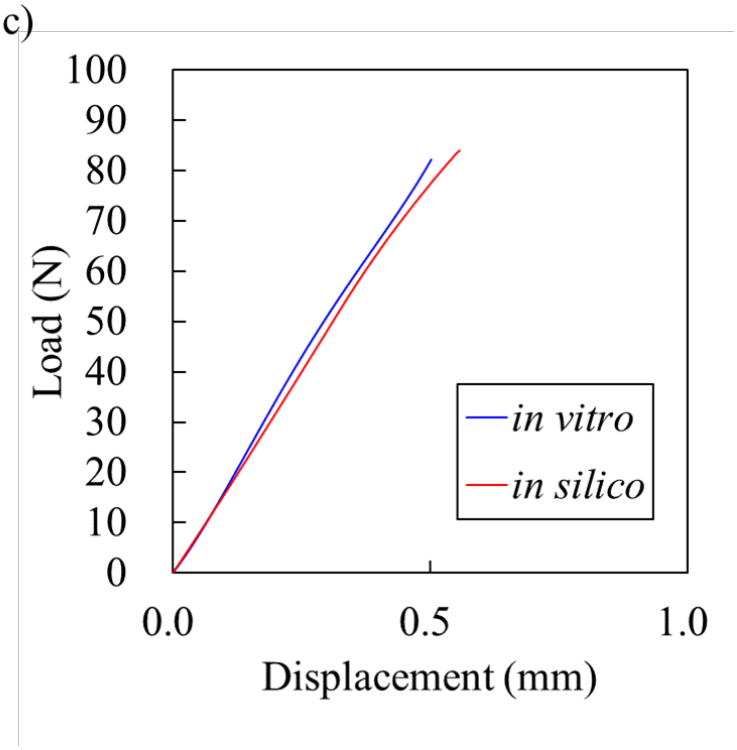


**Fig. 2** Load–displacement curve obtained from *in vitro* / *in silico* three-point bending tests. The *in vitro* curve was obtained by averaging all curves. **a** CS300, **b** AP, **c** GT.

### 3.2 Fracture toughness after *in silico* NTP analysis

The fracture toughness values of CS300, AP, and GT obtained in *in silico* NTP analysis were 5.057 MPa·m$^{1/2}$, 4.193 MPa·m$^{1/2}$, and 4.880 MPa·m$^{1/2}$, respectively. *In silico* load–displacement curves of CS300, AP, and GT obtained in *in silico* NTP analysis are shown in Figure 3. The *in vitro* curve was obtained by averaging all loads at each time point. Both *in vitro* and *in silico* load–displacement curves were significantly correlated (CS300: R=1.0, AP: R=1.0, GT: R=1.0, $p < 0.05$).

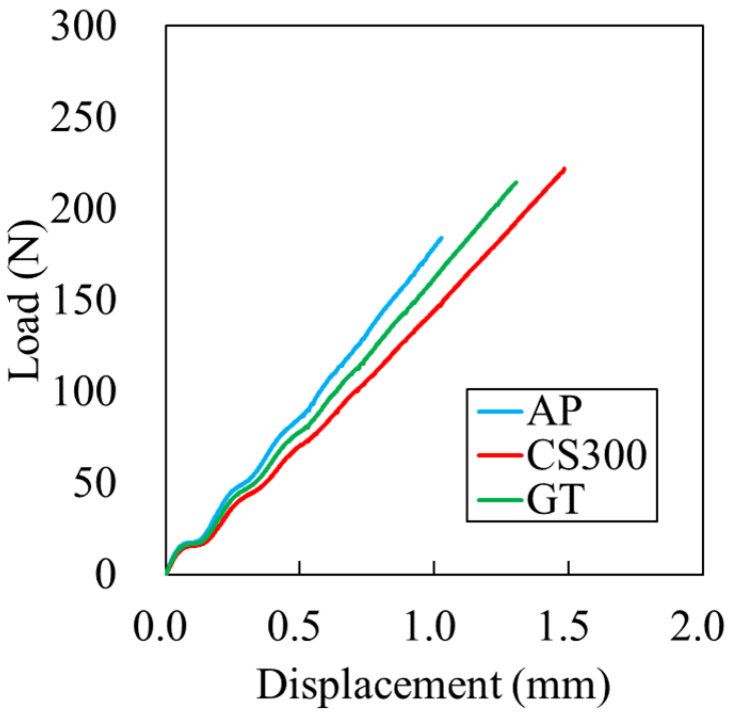


**Fig. 3** Load–displacement curves obtained from *in silico* NTP analysis.

### 3.3 Fractographic analysis

Figure 4 shows SEM images at one side of the fractured surface from the initiation point after NTP tests for CS300 (Fig. 4a), AP (Fig. 4b), and GT (Fig. 4c). White arrows and bold white arrows indicate crack initiation points and the direction of crack propagation. Stable and unstable areas are indicated by yellow lines and were observed throughout the fracture surface of the specimens. The means and standard deviations of the length of the stable region are

shown in Figure 5. There was no significant difference among the three CAD/CAM resin composites ($p = 0.09$).

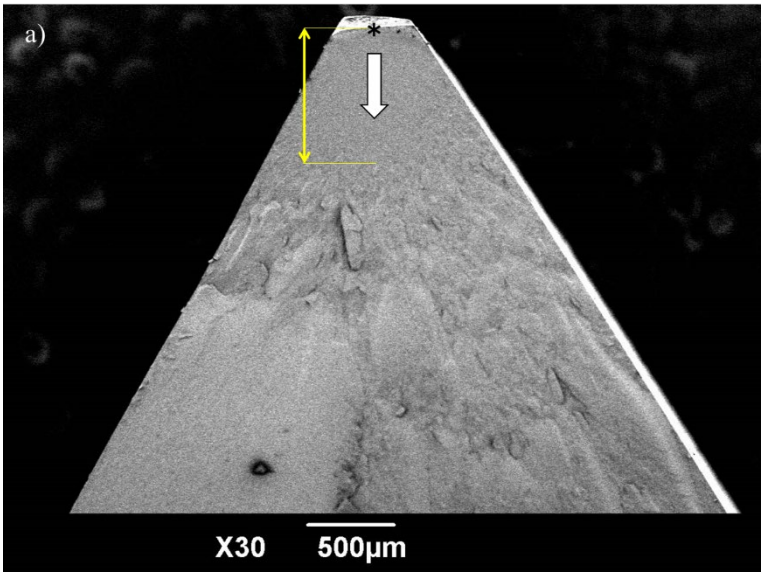


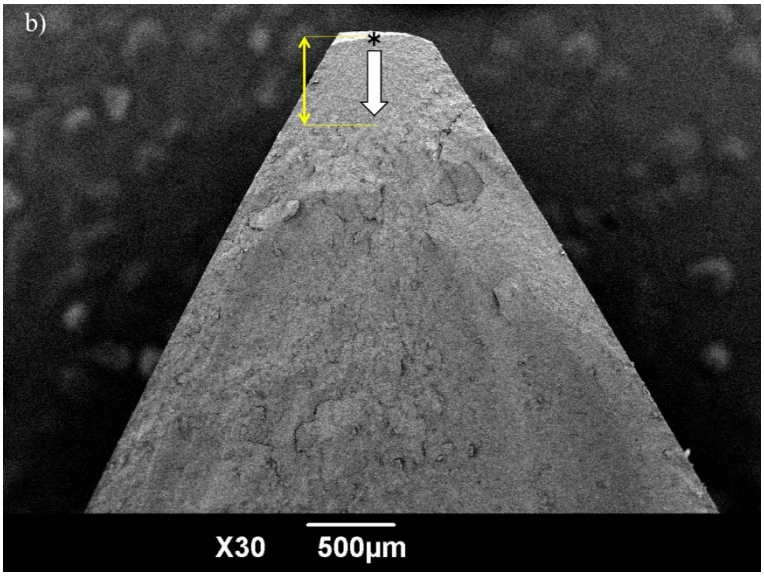

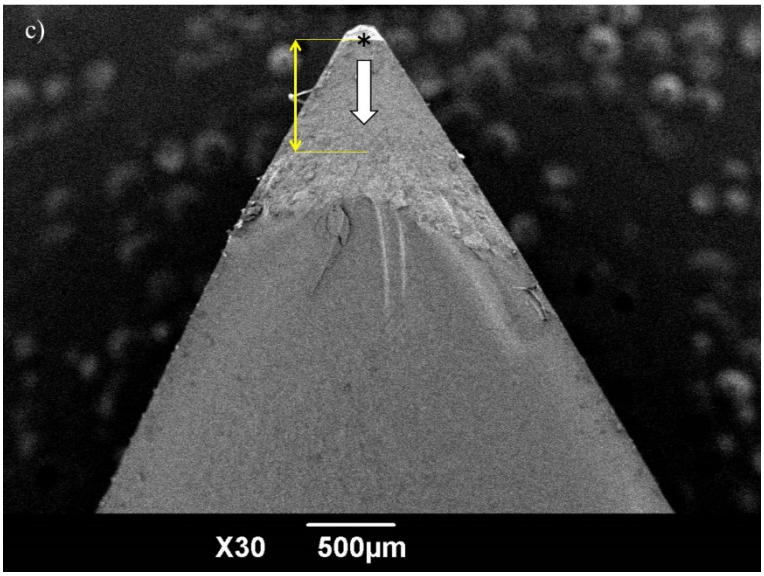


212

213 **Fig. 4** SEM images of fractured surface of specimens after *in vitro* NTP tests. The yellow arrows

214 indicate the length of the stable region. The black asterisks indicate the fracture initiation point.

215 The white arrows indicate the direction of crack propagation. **a** CS300, **b** AP, **c** GT.

216

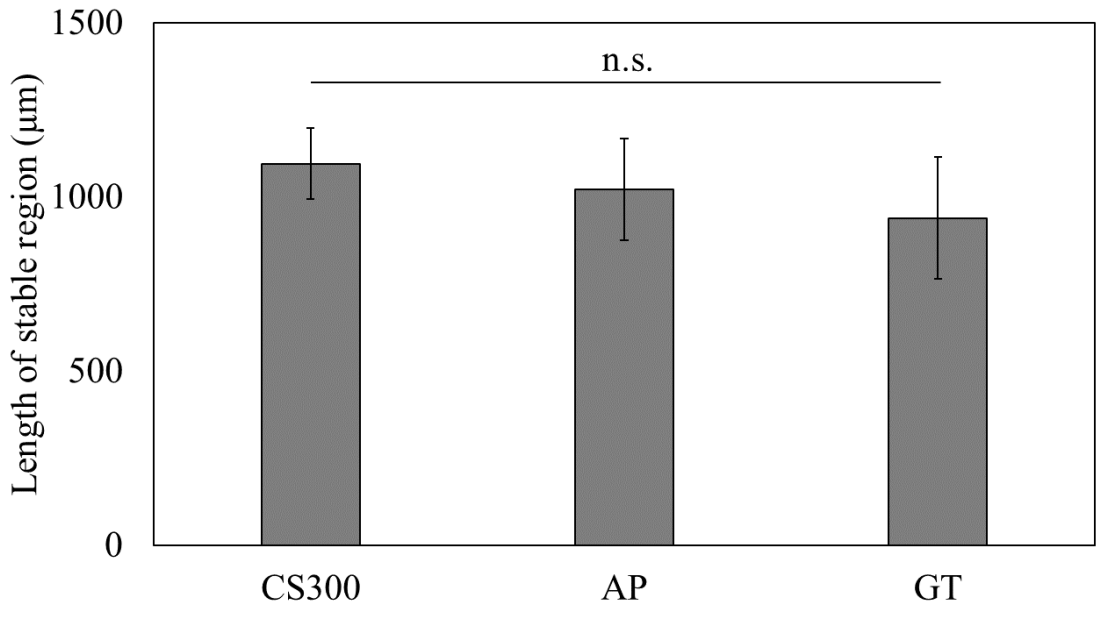


217

218 **Fig. 5** Length of the stable region on the fracture surface after *in vitro* NTP tests.

219

### 3.4 Maximum principal strain distribution in the specimens

Figure 6 shows the maximum principal strain distribution during deformation and after fracture for CS300 (Fig. 6a), AP (Fig. 6b), and GT (Fig. 6c). The tensile strain (positive value of maximum principal strain) is concentrated on the middle edge of the specimens. Fracture was observed at the stretch after exceeding the fracture strain of each material.

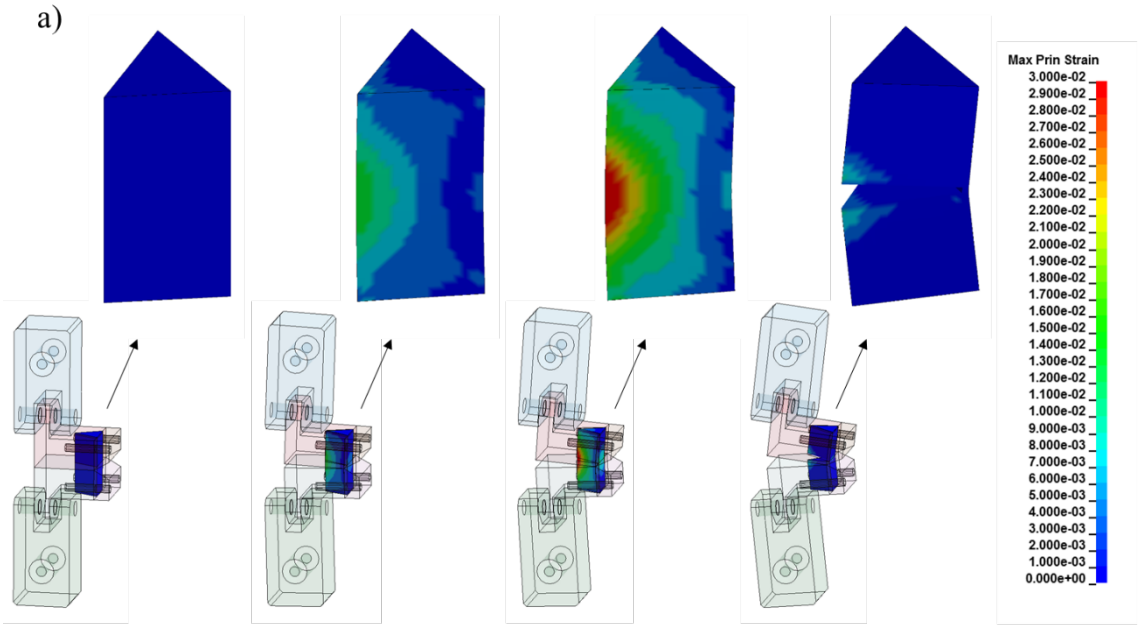

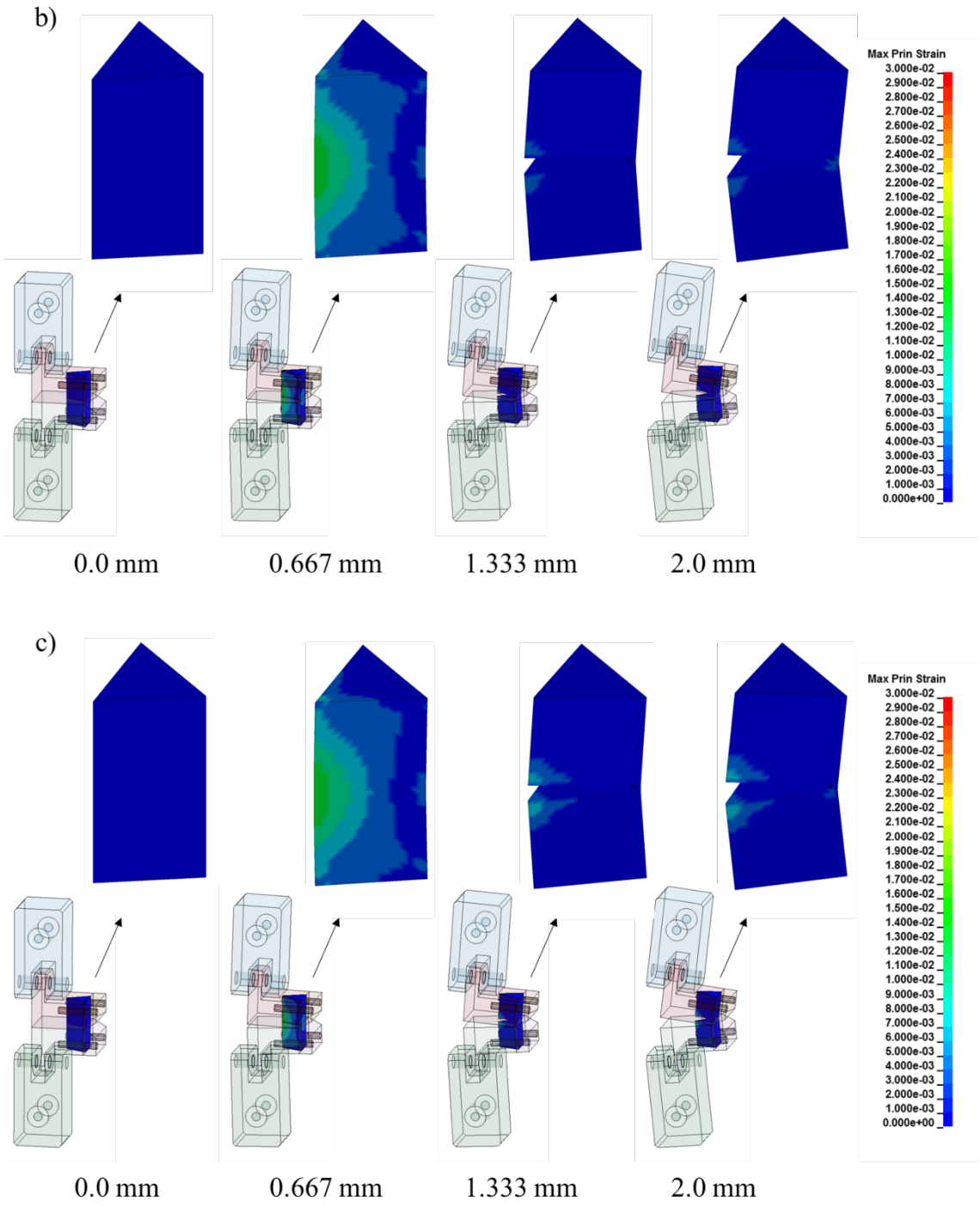


**Fig. 6** Maximum principal strain distribution at each calculation point. 0.0 mm, 0.667 mm, 1.333 mm, and 2.0 mm from left to right. **a** CS300, **b** AP, **c** GT.

## 4. DISCUSSION

An *in silico* three-point bending model was successfully developed and could be used to predict fracture toughness to reflect *in vitro* physical properties obtained from three commercially available CAD/CAM resin composite blocks and demonstrate *in silico* notchless triangular prism (NTP) analysis with those properties. We believe that the *in silico* approach using non-linear dynamic FEA established in this study will become an alternative way to assess fracture toughness related to the longevity of CAD/CAM resin composite crowns without wastage of materials.

The three-point bending tests indicated that the elastic moduli of CS300 and GT were lower than that of AP. From the composition of the materials as shown in Table 1, the inorganic filler content of CS300 and GT was 78 wt% and 75 wt%, respectively, while that of AP was 82 wt%. A lower filler content of resin composites results in a lower flexural modulus (Randolph et al., 2016)/strength (Yamaguchi et al., 2018b) and the volume of the matrix resins must be increased in relation to the amount of fillers. Thus, the lower filler content of CS300 and GT may have resulted in a lower elastic modulus. The elastic modulus is one of the mechanical properties used for evaluating and ranking resin composites (Ilie et al., 2017), and is defined as the initial slope of the stress–strain curve for a given material under loading.

*In silico* three-point bending analysis using non-linear dynamic FEA successfully reflected the *in vitro* testing results. These results suggest that the elastic modulus, density, and fracture strain of each CAD/CAM resin composite could be useful for predicting the flexural modulus and flexural strength. These parameters may be applied to other testing methods such as biaxial flexural tests, four-point bending tests, and fracture toughness tests such as the NTP tests used in this study.

Fracture toughness is an intrinsic material property and is a measure of the energy required to propagate a crack from an existing defect. The NTP test for evaluating fracture toughness adopted in this study was originally proposed by Ruse *et al.* (Ruse et al., 1996). The applications of NTP tests are now expanding to evaluate the interfacial properties of dental materials (Alkadi and Ruse, 2016; Eldafrawy et al., 2018; Mesmar and Ruse, 2019). The *in silico* load–displacement curve of GT in the NTP tests was well matched to the *in vitro* curve. For CS300 and AP, lower fracture loads and displacements were observed *in vitro* compared with *in silico* with statistically significant correlations. One of the reasons for these differences was the construction of jigs for the NTP tests. The specimen cannot be fixed to the jigs without fixation jigs with screws. Even if there are slight differences in the specimen's dimensions at the microscale order, static and dynamic friction properties among the jigs and the specimen will be dramatically changed on the fixation force. Thus, the *in silico* approach could avoid

these frictional effects and allow direct comparison by focusing on the different material composition of each CAD/CAM resin composite block.

The SEM images showed that both stable and unstable areas (Alkadi and Ruse, 2016) resulted in mode I fracture (the tensile loading direction is vertical to the fracture surface). The length of the stable area from the crack initiation point to the boundary between the stable and unstable areas was not significantly different among the CAD/CAM resin composites, while a shorter length of stable area has been reported in lithium disilicate glass ceramics (Alkadi and Ruse, 2016; Mesmar and Ruse, 2019). These results suggest that CAD/CAM resin composites inhibit crack propagation to a greater degree than lithium disilicate glass ceramics.

Stable and unstable areas were not observable on the *in silico* models because the mesh size of 0.3 mm was too large to represent the nano/microstructural details of the fractured surface. The calculation cost would need to be increased corresponding to a higher resolution mesh. Multi-scale analysis may be helpful to find the crack initiation point at the nano/microscale level (Takano et al., 2010; Takano et al., 2003; Yamaguchi et al., 2017). *In silico* nanoscale models of CAD/CAM resin composites blocks have been developed using electron microscopy with cryo-stage and focused ion beam (Lee et al., 2019). The combination of non-linear dynamic FEA and multi-scale analysis using nanoscale models may accelerate

284 elucidation of the fracture mechanism and the development of new materials with greater
285 longevity.

286 While of CAD/CAM resin composites exhibit greater fracture toughness, hydrolysis of
287 the silane coupling and matrix resins in the oral environment (Drummond, 2008; Kusuma
288 Yulianto et al., 2019) should be considered in future studies. Nanoscale models containing a
289 silane coupling layer are under development for investigating the influence on the mechanical
290 properties of CAD/CAM resin composites.

291

## 5. CONCLUSIONS

The *in silico* approach established in this study acceptably reflected the *in vitro* physical properties and will be useful for assessing fracture toughness related to the longevity of CAD/CAM resin composites without wastage of materials.

297 **ACKNOWLEDGEMENTS**

298 This research was supported by a Grant-in-Aid for Scientific Research (No.

299 JP19K10244) from the Japan Society for the Promotion of Science (JSPS). We thank Helen

300 Jeays, BDSc AE, from Edanz Group (www.edanzediting.com/ac) for editing a draft of this

301 manuscript.

302

## REFERENCES


Alkadi, L., Ruse, N.D., 2016. Fracture toughness of two lithium disilicate dental glass ceramics. J Prosthet Dent 116, 591-596.

Ausiello, P., Rengo, S., Davidson, C.L., Watts, D.C., 2004. Stress distributions in adhesively cemented ceramic and resin-composite Class II inlay restorations: a 3D-FEA study. Dent Mater 20, 862-872.

Coelho, P.G., Calamia, C., Harsono, M., Thompson, V.P., Silva, N.R., 2008. Laboratory and FEA evaluation of dentin-to-composite bonding as a function adhesive layer thickness. Dent Mater 24, 1297-1303.

Coldea, A., Swain, M.V., Thiel, N., 2013a. In-vitro strength degradation of dental ceramics and novel PICN material by sharp indentation. J Mech Behav Biomed Mater 26, 34-42.

Coldea, A., Swain, M.V., Thiel, N., 2013b. Mechanical properties of polymer-infiltrated-ceramic-network materials. Dent Mater 29, 419-426.

Dal Piva, A.M.O., Tribst, J.P.M., Borges, A.L.S., Souza, R., Bottino, M.A., 2018. CAD-FEA modeling and analysis of different full crown monolithic restorations. Dent Mater 34, 1342-1350.

Della Bona, A., Borba, M., Benetti, P., Duan, Y., Griggs, J.A., 2013. Three-dimensional finite element modelling of all-ceramic restorations based on micro-CT. J Dent 41, 412-419.

321 Drummond, J.L., 2008. Degradation, fatigue, and failure of resin dental composite materials. J
322 Dent Res 87, 710-719.
323 Eldafrawy, M., Ebroin, M.G., Gailly, P.A., Nguyen, J.F., Sadoun, M.J., Mainjot, A.K., 2018.
324 Bonding to CAD-CAM Composites: An Interfacial Fracture Toughness Approach. J Dent Res
325 97, 60-67.
326 Ferracane, J.L., 2011. Resin composite--state of the art. Dent Mater 27, 29-38.
327 Fujishima, A., Ferracane, J.L., 1996. Comparison of four modes of fracture toughness testing
328 for dental composites. Dent Mater 12, 38-43.
329 Greaves, G.N., Greer, A.L., Lakes, R.S., Rouxel, T., 2011. Poisson's ratio and modern materials.
330 Nat Mater 10, 823-837.
331 Heintze, S.D., Ilie, N., Hickel, R., Reis, A., Loguercio, A., Rousson, V., 2017. Laboratory
332 mechanical parameters of composite resins and their relation to fractures and wear in clinical
333 trials-A systematic review. Dent Mater 33, e101-e114.
334 Ilie, N., Hickel, R., Valceanu, A.S., Huth, K.C., 2012. Fracture toughness of dental restorative
335 materials. Clin Oral Investig 16, 489-498.
336 Ilie, N., Hilton, T.J., Heintze, S.D., Hickel, R., Watts, D.C., Silikas, N., Stansbury, J.W.,
337 Cadenaro, M., Ferracane, J.L., 2017. Academy of Dental Materials guidance-Resin composites:
338 Part I-Mechanical properties. Dent Mater 33, 880-894.

339 Kusuma Yulianto, H.D., Rinastiti, M., Cune, M.S., de Haan-Visser, W., Atema-Smit, J.,
340 Busscher, H.J., van der Mei, H.C., 2019. Biofilm composition and composite degradation
341 during intra-oral wear. Dent Mater.
342 Lee, C., Yamaguchi, S., Ohta, K., Imazato, S., 2019. Mechanical properties of computer-aided
343 design/computer-aided manufacturing resin composites assuming perfect silane coupling using
344 in silico homogenization of cryo-electron microscopy images. J Prosthodont Res 63, 90-94.
345 Mesmar, S., Ruse, N.D., 2019. Interfacial Fracture Toughness of Adhesive Resin Cement-
346 Lithium-Disilicate/Resin-Composite Blocks. J Prosthodont 28, e243-e251.
347 Nguyen, J.F., Migonney, V., Ruse, N.D., Sadoun, M., 2012. Resin composite blocks via high-
348 pressure high-temperature polymerization. Dent Mater 28, 529-534.
349 Nguyen, J.F., Migonney, V., Ruse, N.D., Sadoun, M., 2013. Properties of experimental
350 urethane dimethacrylate-based dental resin composite blocks obtained via thermo-
351 polymerization under high pressure. Dent Mater 29, 535-541.
352 Okada, K., Kameya, T., Ishino, H., Hayakawa, T., 2014. A novel technique for preparing dental
353 CAD/CAM composite resin blocks using the filler press and monomer infiltration method. Dent
354 Mater J 33, 203-209.

355 Ornaghi, B.P., Meier, M.M., Lohbauer, U., Braga, R.R., 2014. Fracture toughness and cyclic
356 fatigue resistance of resin composites with different filler size distributions. Dent Mater 30,
357 742-751.
358 Randolph, L.D., Palin, W.M., Leloup, G., Leprince, J.G., 2016. Filler characteristics of modern
359 dental resin composites and their influence on physico-mechanical properties. Dental Materials
360 32, 1586-1599.
361 Ruse, N.D., Sadoun, M.J., 2014. Resin-composite blocks for dental CAD/CAM applications. J
362 Dent Res 93, 1232-1234.
363 Ruse, N.D., Troczynski, T., MacEntee, M.I., Feduik, D., 1996. Novel fracture toughness test
364 using a notchless triangular prism (NTP) specimen. J Biomed Mater Res 31, 457-463.
365 Takano, N., Fukasawa, K., Nishiyabu, K., 2010. Structural strength prediction for porous
366 titanium based on micro-stress concentration by micro-CT image-based multiscale simulation.
367 Int J Mech Sci 52, 229-235.
368 Takano, N., Zako, M., Kubo, F., Kimura, K., 2003. Microstructure-based stress analysis and
369 evaluation for porous ceramics by homogenization method with digital image-based modeling.
370 Int J Solids Struct 40, 1225-1242.
371 Tantbirojn, D., Versluis, A., Cheng, Y.S., Douglas, W.H., 2003. Fracture toughness and
372 microhardness of a composite: do they correlate? J Dent 31, 89-95.

373 Yamaguchi, S., Inoue, S., Sakai, T., Abe, T., Kitagawa, H., Imazato, S., 2017. Multi-scale
374 analysis of the effect of nano-filler particle diameter on the physical properties of CAD/CAM
375 composite resin blocks. Comput Methods Biomech Biomed Engin 20, 714-719.
376 Yamaguchi, S., Kani, R., Kawakami, K., Tsuji, M., Inoue, S., Lee, C., Kiba, W., Imazato, S.,
377 2018a. Fatigue behavior and crack initiation of CAD/CAM resin composite molar crowns. Dent
378 Mater 34, 1578-1584.
379 Yamaguchi, S., Mehdawi, I.M., Sakai, T., Abe, T., Inoue, S., Imazato, S., 2018b. In vitro/in
380 silico investigation of failure criteria to predict flexural strength of composite resins. Dent
381 Mater J 37, 152-156.
382 Yamaguchi, S., Tsutsui, K., Satake, K., Morikawa, S., Shirai, Y., Tanaka, H.T., 2014. Dynamic
383 analysis of a needle insertion for soft materials: Arbitrary Lagrangian-Eulerian-based three-
384 dimensional finite element analysis. Comput Biol Med 53, 42-47.
385 Yamanishi, Y., Yamaguchi, S., Imazato, S., Nakano, T., Yatani, H., 2014. Effects of the implant
386 design on peri-implant bone stress and abutment micromovement: three-dimensional finite
387 element analysis of original computer-aided design models. J Periodontol 85, e333-338.
388
389